

Supplement of Atmos. Meas. Tech., 13, 1129–1155, 2020
<https://doi.org/10.5194/amt-13-1129-2020-supplement>
© Author(s) 2020. This work is distributed under
the Creative Commons Attribution 4.0 License.



Supplement of

Validation of MAX-DOAS retrievals of aerosol extinction, SO₂, and NO₂ through comparison with lidar, sun photometer, active DOAS, and aircraft measurements in the Athabasca oil sands region

Zoë Y. W. Davis et al.

Correspondence to: Zoë Y. W. Davis (zoeywd@yorku.ca)

The copyright of individual parts of the supplement might differ from the CC BY 4.0 License.

Supplemental to Validation of MAX-DOAS retrievals of aerosol extinction, SO₂ and NO₂ through comparison with lidar, sun photometer, Active-DOAS and aircraft measurements in the Athabasca Oil Sands Region.

Section 1 Emissions of NO₂ and SO₂ from AOSR Industrial Facilities

Table S1 Annual Emissions NO₂ in kilotonnes from select facilities.

Facility	NPRI 2013	Off-road vehicle & tail-pipe emissions (Zhang et al., 2018) from 2010	Stack & area sources (Zhang et al., 2018) (2012-2013 period)
Syncrude Mildred Lake Plant	14	8.0	14
Suncor Millennium Plant/Steepbank	8	10.7	11.5
Shell Muskeg River/Jackpine	1.3	7.0	0.7
CNRL Horizon	1.5	5.6	1.8
Imperial Oil Kearl	0.3	1.3	0

Table S2 Annual Emissions SO₂ in kilotonnes from select facilities.

Facility	NPRI 2013	Off-road vehicle & tail-pipe emissions (Zhang et al., 2018) from 2010	Stack & area sources (Zhang et al., 2018) (2012-2013 period)
Syncrude Mildred Lake Plant	63	0.36	77
Suncor Millennium Plant/Steepbank	14	0.06	21
Shell Muskeg River/Jackpine	0	0.13	0
CNRL Horizon	4	0.07	6.5
Imperial Oil Kearl	0	0.03	0



Figure S1 The MAX-DOAS instrument mounted at 5 m a.g.l. (left) at Fort McKay South and the view South of the instrument.

Section 2 Additional Information on MAX-DOAS Spectral Fitting

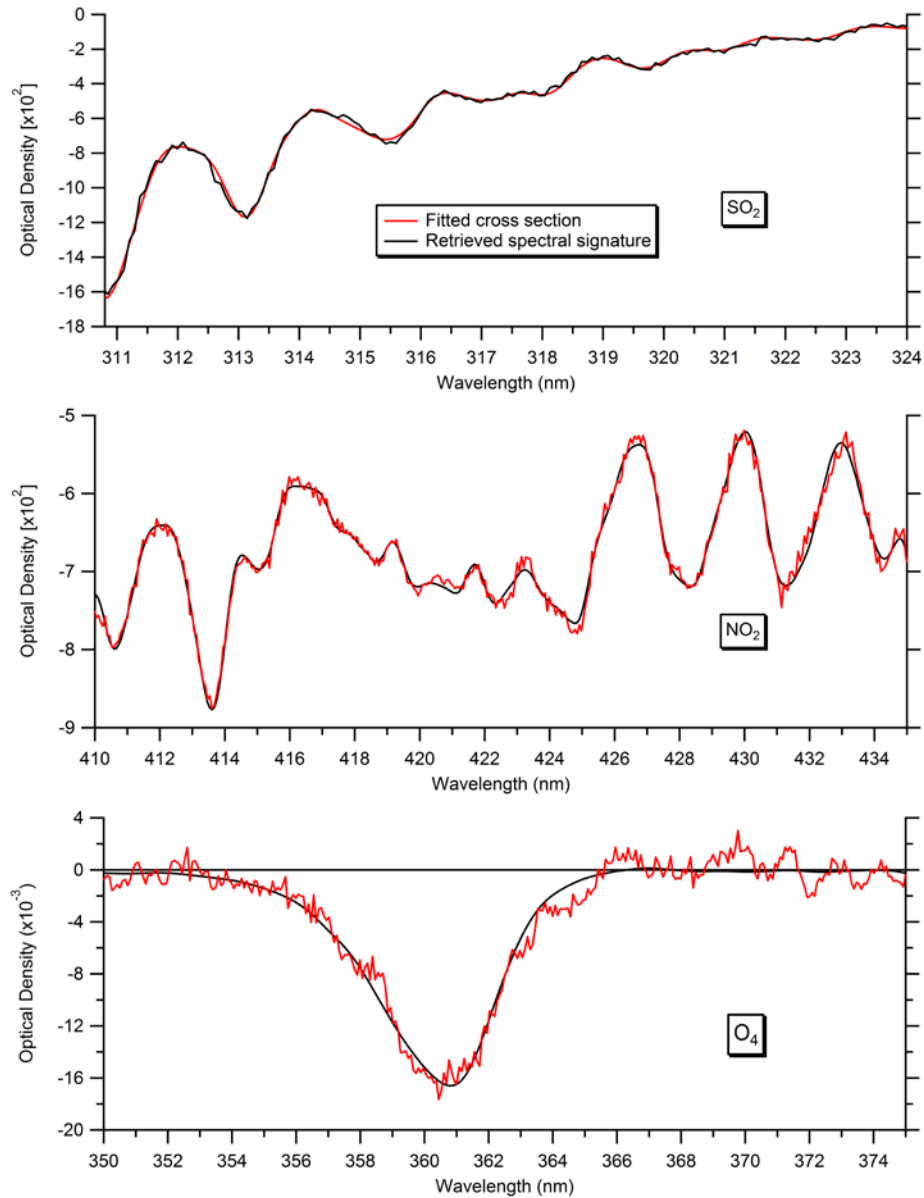


Figure S2 Examples of spectral retrievals of SO₂, NO₂ and O₄. Retrieved dSCDs were $5.79(\pm 0.09) \times 10^{17}$ molec cm⁻², $1.2(\pm 0.01) \times 10^{17}$ molec cm⁻², and $3.96(\pm 0.08) \times 10^{43}$ molec cm⁻², respectively. The spectra were measured under clear sky conditions at 2° in 2013 at 22:37 UTC on Aug 23 and 18:34 UTC on Sep 04, respectively.

SO₂ Spectral Fitting Experiments with Calibration Gas Cell

A SO₂ gas cell with a slant column density (SCD) of $2.2e^{17}$ ($\pm 10\%$) molecules cm⁻² was placed inside the MAX-DOAS telescope tube. Scattered solar light spectra were recorded around solar noon at viewing elevation angles of 2°, 4°, 8°, 30° and 90° above the horizon, followed by a 90° measurement without the gas cell. This second zenith measurement was used as the FRS. Active-DOAS measurements of the SO₂ gas cell confirmed the SCD. dSCDs of SO₂ were fit in DOASIS with varying fitting windows using a lower limit range of 303-318 nm and an upper limit range of 309-340 nm in ~0.3 nm increments. The fit components can be found in Table 2.

Fitting SO₂ in the measured wavelength region is challenging because the SO₂ absorption features (Fig. S3) are strongest where the measured light intensity was small, and the influence of stray light can be large. Increasing O₃ absorption at decreasing wavelengths approaching 300 nm reduces the spectral signal. The lower limit wavelength of the fitting window must balance including strong SO₂ features and enough signal intensity. The upper limit wavelength should ensure that the fitting window includes as many SO₂ absorption features as possible while excluding wavelengths where SO₂ absorption features are so weak that degrees of freedom and fitting uncertainty are increased.

dSCD of SO₂ fitted from the spectra measured at elevation angles closer to horizon-pointing exhibited fewer wavelength fitting windows where the fitted dSCD was within $\pm 15\%$ of the expected value. Spectra measured at lower elevation angles had less UV signal because the longer light path lengths closer to the ground experience more Rayleigh scattering that preferentially scattered away shorter wavelengths. Since the visible light intensity remains the same and is a source of stray light, the reduced UV signal increased the impact of stray light on the dSCD (signal to noise ratio decreases). Stray light artificially increases the measured intensity and tends to cause underestimation of the retrieved dSCD.

Stray light has the largest impact on the signal at the lowest wavelengths where the measured intensity was the lowest. Stray light interference is apparent in the frequent underestimation of the dSCD for the 2° spectrum with fitting windows with lower limits <307 nm (gray datapoints in Fig. S4). The dSCDs were often >15% less than the expected value for fitting windows with a lower limit <308 nm, particularly for the lower elevation angles. The fitted dSCD was sensitive to small changes in the fitting window for lower limits <308 nm and upper limit <330 nm, changing up to ~20% change for a 0.5 nm difference in the lower limit (Figs. S4 & S5). The fitted dSCD is inversely proportion to the SO₂ absorption cross section (Fig S4). When the strongest SO₂ absorption feature included in the fit was an absorption maximum, the measured intensity in lowest wavelength region was even further reduced, leading to up to a 25% reduction in the dSCD compared to a window where the adjacent absorption minimum was the strongest feature included (Fig. S5). This result implies that small errors in the wavelength calibration or wavelength shift could significantly deviate the dSCD from the true value. dSCDs exhibited less dependence on the lower limit for windows with lower limit wavelengths of 310.4-311 nm due to increased signal intensity. For lower limit wavelengths >312 nm, the SO₂ absorption features are substantially weaker, leading to dSCDs that tended to be >15% larger than the expected value and varied significantly with relatively small changes in higher limit

wavelength (Fig. S4). Since the SO₂ absorption features after 324 nm are very weak, the fitting range upper limit was set to 324 nm.

Based on these results, an SO₂ fitting range of 310.5-324 nm was chosen for this instrument.

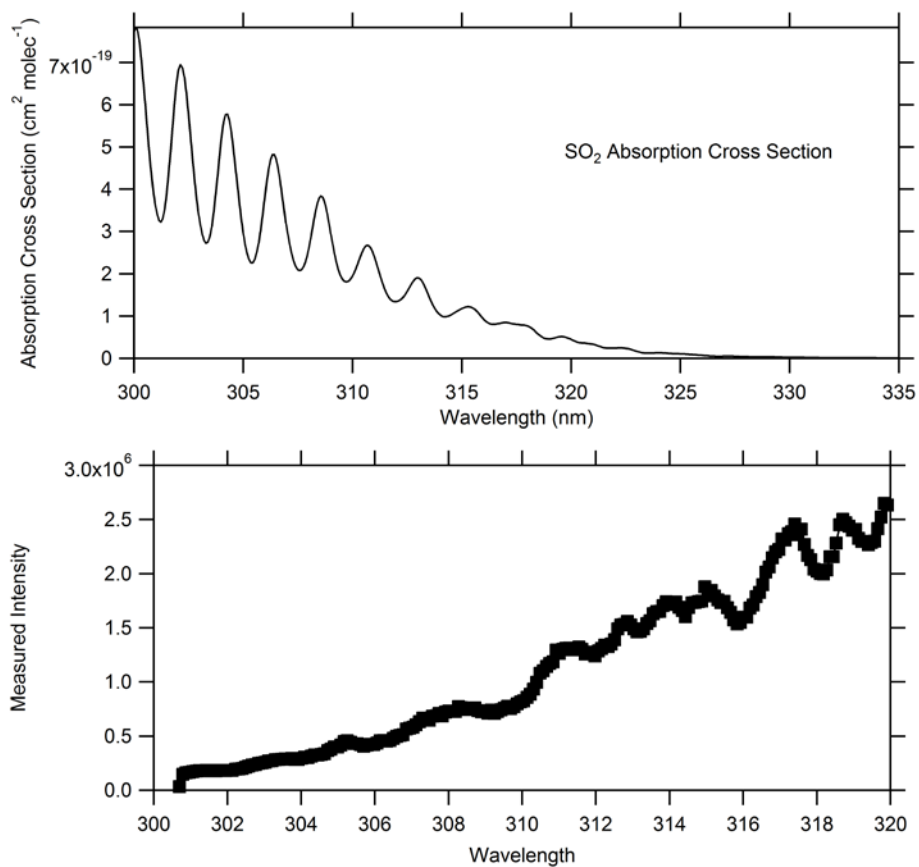


Figure S3 SO₂ Absorption Cross Section (top) and Measured Intensity from the 2^o Spectrum from 300-320 nm (bottom).

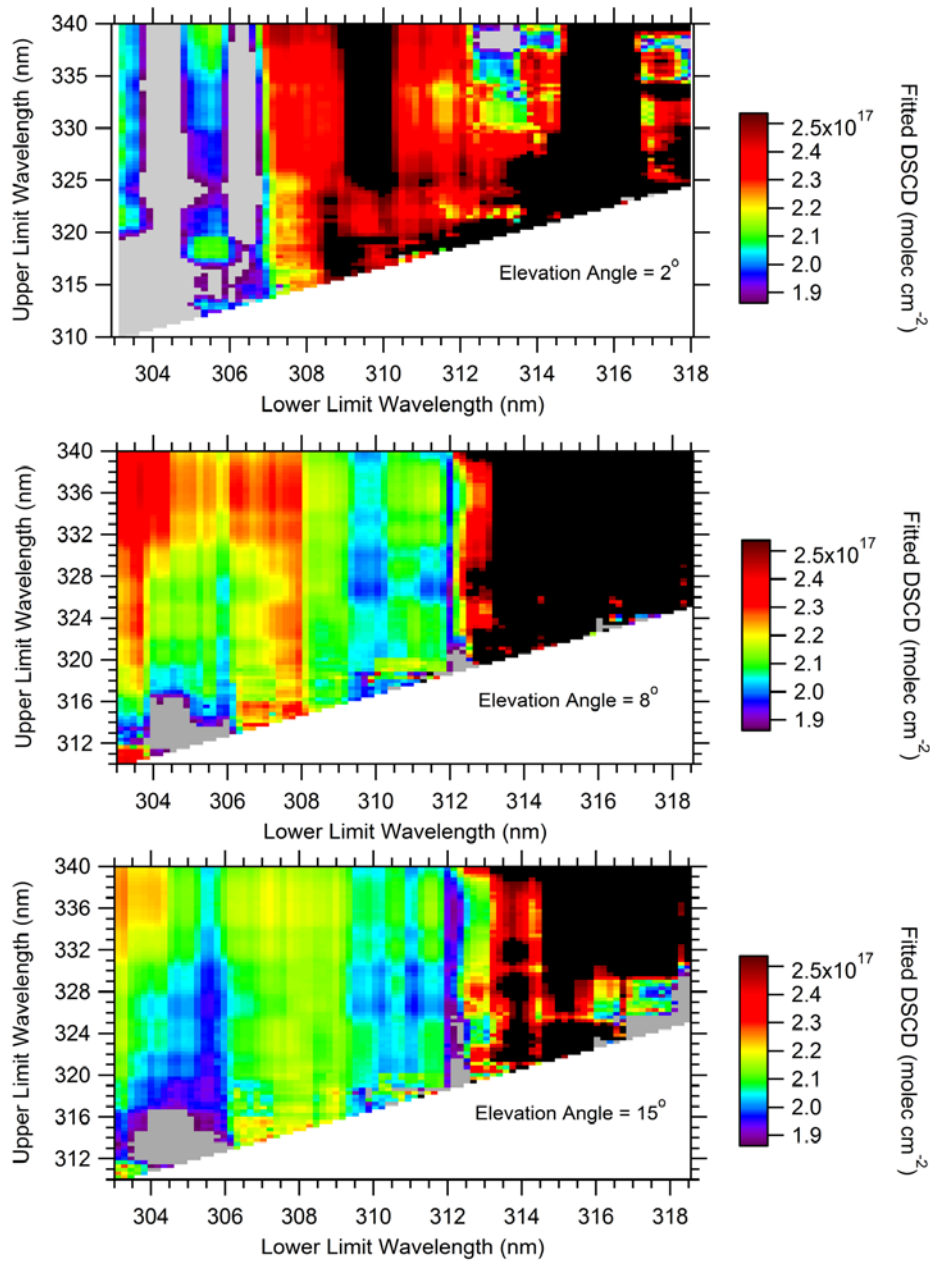


Figure S4 dSCDs of SO_2 , 2×10^{17} molecules cm^{-2} gas cell using varying spectral fitting ranges. Gray and black datapoints indicate that the fitted dSCD was 15% less than and greater than 2.2×10^{17} molec cm^{-2} , respectively.

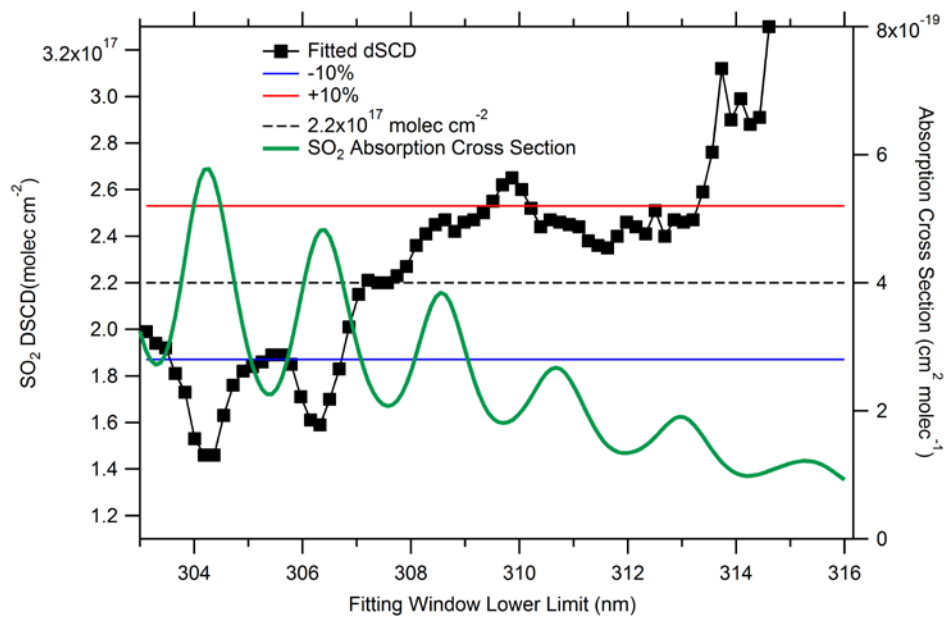


Figure S5 Fitted dSCD of SO₂ with fitting window upper limit of 320 nm from 2° Spectrum using a 2.2x10¹⁷ molec cm⁻² gas cell (black trace) and SO₂ absorption cross section degraded to the spectrometer's resolution (green trace).

Section 3 Lidar S-ratio Measurements in the AOSR

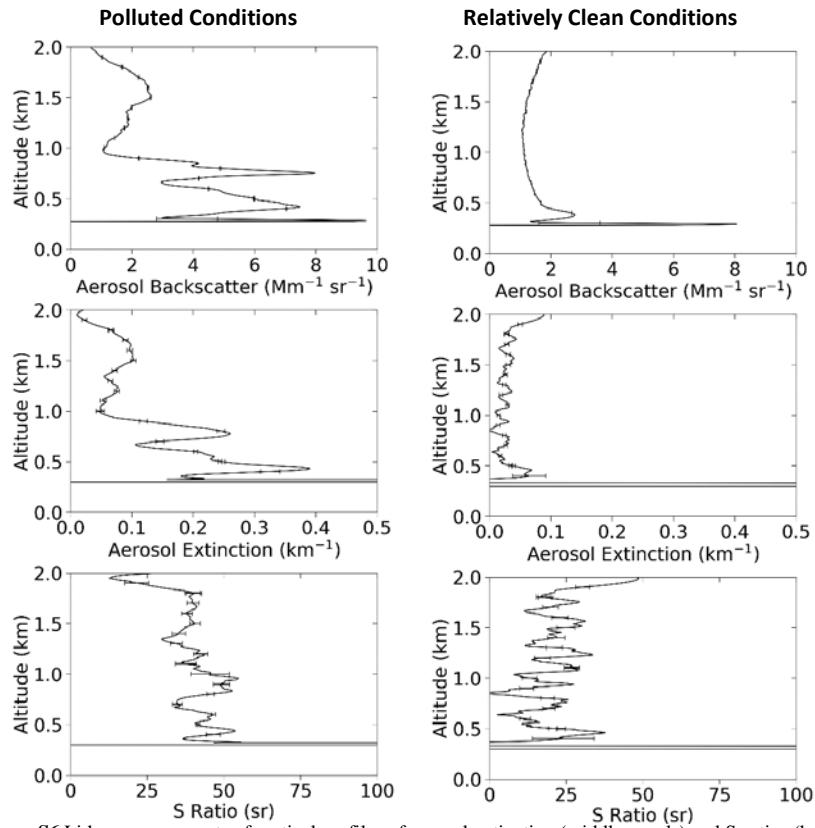


Figure S6 Lidar measurements of vertical profiles of aerosol extinction (middle panels) and S-ratios (bottom panels) under polluted conditions (left column) and relatively clean conditions (right column) at Oski-Ôtin in 2018.

Section 4 Linear Regression Statistics

Table S3 Aug 23 AOD Linear Regressions.

Y	MAX-DOAS AOD	MAX-DOAS AOD	MAX-DOAS AOD	MAX-DOAS AOD	AERONET AOD -30 mins	AERONET AOD -30 mins
X	AERONET AOD -30mins	AERONET AOD	Lidar AOD S=44 sr in plume	Lidar AOD S=25 sr	Lidar S=44 sr	Lidar S=25 sr
Slope	0.98±0.02	1.03±0.01	1.15±0.02	2.18±0.03	1.08±0.02	2.18±0.01
Intercept	-0.08±0.00	-0.07±0.00	-0.01±0.00	-0.06±0.00	0.07±0.00	0.03±0.01
R ²	0.92	0.80	0.97	0.97	0.98	0.96
N	21	23	21	24	22	22

Table S4 Aug 23 trace-gas linear regressions. *Denotes the matrix was near-singular or badly conditioned; statistical results may be inaccurate.

Y	MAX-DOAS SO ₂ VCD	MAX-DOAS SO ₂ VCD	MAX-DOAS NO ₂ VCD	MAX-DOAS NO ₂ VCD	WBEA Fort McKay South SO ₂ mixing ratio	WBEA Fort McKay South NO ₂ mixing ratio
X	Pandora SO ₂ VCD	Pandora SO ₂ VCD -30mins	Pandora NO ₂ VCD	Pandora NO ₂ VCD -30 mins	WBEA Oski-Ôtin SO ₂ mixing ratio -30 mins	WBEA Oski-Ôtin NO ₂ mixing ratio -30 mins
Slope	*1.61±0.10	*1.55±0.07	*2.03±0.07	*2.20±0.07	1.42±0.05	1.93±0.07
Intercept	*1.50x10 ¹⁶ ±0.25x10 ¹⁶	*1.16x10 ¹⁶ ±0.24x10 ¹⁶	*-4.56 ¹⁵ ±0.51x10 ¹⁵	*-6.36x10 ¹⁵ ±0.56x10 ¹⁵	0.50±0.01	1.95±0.52
R ²	0.51	0.82	0.68	0.87	0.91	0.61
N	24	23	24	23	109	109

Table S5 Sep 03 AOD and trace-gas linear regressions for data from 11:30 to 18:00. ^Denotes that one or both variables exhibited little variation; the R² is not interpretable.

Y	MAX-DOAS AOD	MAX-DOAS AOD	AERONET AOD	MAX-DOAS SO ₂ VCD	MAX-DOAS NO ₂ VCD	WBEA Fort McKay South SO ₂ mixing ratio	WBEA Fort McKay South NO ₂ mixing ratio
X	AERONET AOD	Lidar AOD	Lidar AOD	Pandora SO ₂ VCD	Pandora NO ₂ VCD	WBEA Oski-Ötin SO ₂ mixing ratio	WBEA Oski-Ötin NO ₂ mixing ratio
Slope	0.01±0.01	-0.59±0.36	3.30±0.48	5.27±2.9	-0.19±0.64	0.97±0.10	0.61±0.08
Intercept	-0.01±0.01	0.12±0.02	-0.08±0.03	-1.5x10 ¹⁷ ±1.11x10 ¹⁷	1.38x10 ¹⁶ ±0.44x10 ¹⁵	-1.91±1.99	1.82±0.53
R ²	^0.02	^0.05	^0.47	^0.01	^0.00	0.53	0.38
N	16	16	16	13	12	80	80

Table S6 Sep 04 AOD and trace-gas linear regressions. *Denotes the matrix was near-singular or badly conditioned; statistical results may be inaccurate. . ^Denotes that one or both variables exhibited little variation; the R² is not interpretable.

Y	MAX-DOAS AOD	MAX-DOAS AOD	AERONET AOD	MAX-DOAS SO ₂ VCD	MAX-DOAS NO ₂	WBEA Fort McKay South SO ₂ mixing ratio	WBEA Fort McKay South NO ₂ mixing ratio
X	AERONET AOD	Lidar AOD	Lidar AOD	Pandora SO ₂ VCD	Pandora NO ₂ VCD	WBEA Bertha Ganterfort SO ₂ mixing ratio	WBEA Bertha Ganterfort NO ₂ mixing ratio
Slope	0.39±0.031	0.78±0.08	2.23±0.07	1.10±0.33	*0.95±0.07	0.58±0.04	0.86±0.02
Intercept	-0.01±0.01	0.00±0.01	0.02±0.01	4.62x10 ¹⁵ ±2.40x10 ¹⁵	*9.44x10 ¹⁴ ±3.93x10 ¹⁴	1.77±0.25	1.00±0.16
R ²	0.31	0.20	0.91	0.51	0.85	0.7	0.92
N	25	25	25	25	25	108	108

Table S7 Sep 05 AOD linear regressions.

Y	MAX-DOAS AOD	MAX-DOAS AOD	AERONET AOD
X	AERONET AOD	Lidar AOD	Lidar AOD
Slope	1.04±0.08	2.94±0.38	3.24±0.15
Intercept	-0.08±0.01	-0.10±0.02	-0.03±0.01
R ²	0.77	0.51	0.89
N	26	20	20

Table S8 Sep 06 AOD linear regressions. *Denotes the matrix was near-singular or badly conditioned; statistical results may be inaccurate. ^Denotes that one or both variables exhibited little variation; the R² is not interpretable.

Y	MAX-DOAS AOD	MAX-DOAS AOD	AERONET AOD 361
X	AERONET AOD	Lidar AOD	Lidar AOD
Slope	*-2.01±0.93	5.56±1.27	-2.33±0.73
Intercept	0.24±0.09	-0.21±0.06	0.20±0.03
R ²	^0.02	0.02	^0.08
N	24	23	23

Table S9 Sep 07 AOD and trace-gas linear regressions. *Denotes the matrix was near-singular or badly conditioned; statistical results may be inaccurate.

Y	MAX-DOAS AOD	MAX-DOAS AOD	AERONET AOD	MAX-DOAS SO ₂ VCD	MAX-DOAS NO ₂ VCD	WBEA Fort McKay South SO ₂ mixing ratio	WBEA Fort McKay South NO ₂ mixing ratio
X	AERONET AOD	Lidar AOD	Lidar AOD	Pandora SO ₂ VCD	Pandora NO ₂ VCD	WBEA Bertha Ganterfort SO ₂ mixing ratio	WBEA Bertha Ganterfort NO ₂ mixing ratio
Slope	0.73±0.06	1.83±0.13	2.34±0.10	*1.48x10 ¹⁴ ±1.48x10 ¹⁴	*1.53±3.3	0.99±0.07	1.06±0.03
Intercept	-0.03±0.01	-0.04±0.01	0.00±0.00	*-1.09x10 ³⁰ ±1.049x10 ³⁰	*4.10x10 ¹⁵ ±1.75x10 ¹⁶	-0.04±0.36	1.05±0.23
R ²	0.64	0.67	0.55	^0.00	^0.05	0.64	0.90
N	26	26	26	26	26	108	108

Section 5 Example of Averaging Kernel Matrix from MAX-DOAS Optimal Estimation Retrieval

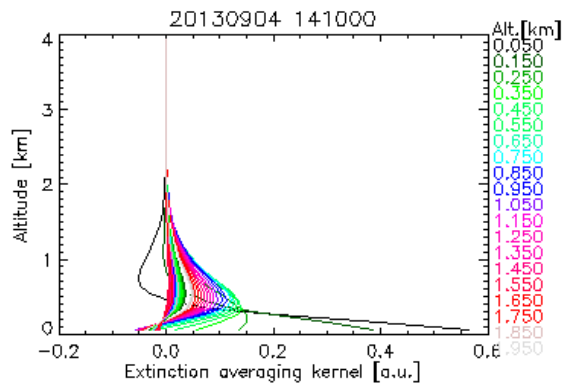


Figure S7 Example of typical averaging kernels from the MAX-DOAS Sep 04 14:10 retrieval of aerosol extinction.

Section 6 Detailed Plots of Selected Lidar Data

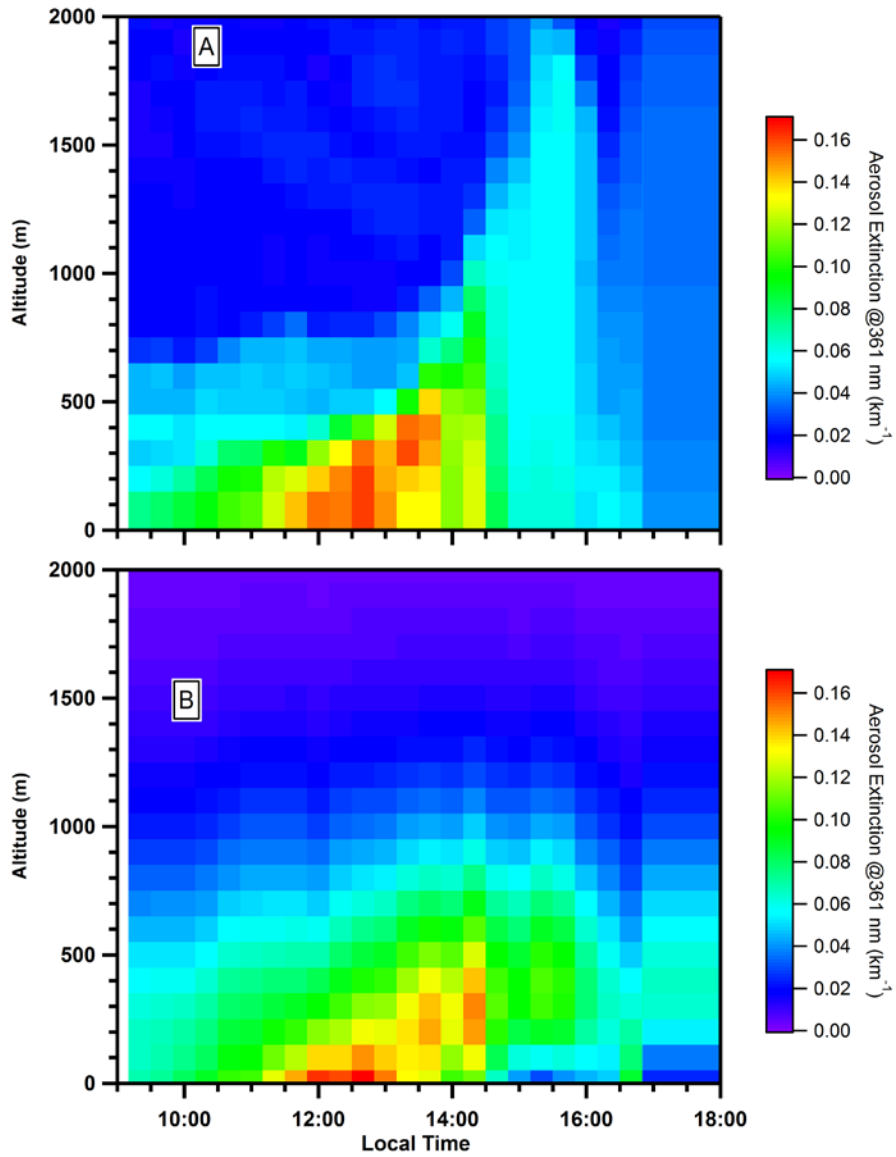


Figure S8 Detail of Sep 04 averaged (A) and smoothed (B) lidar profiles from 0-2 km.

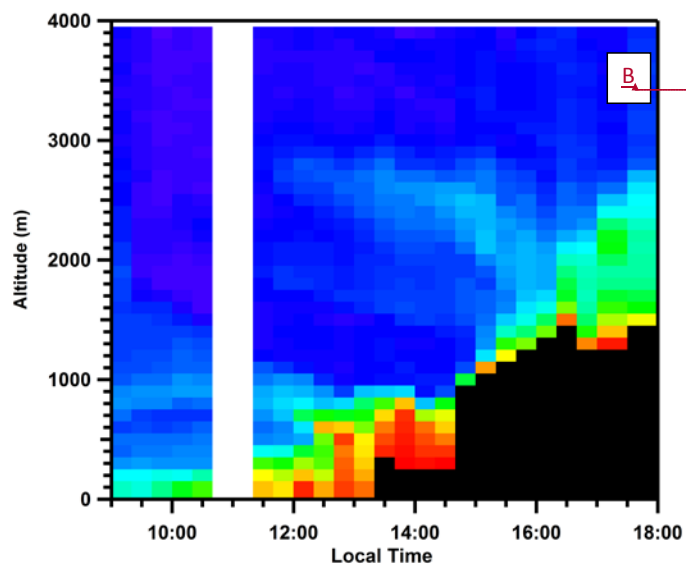
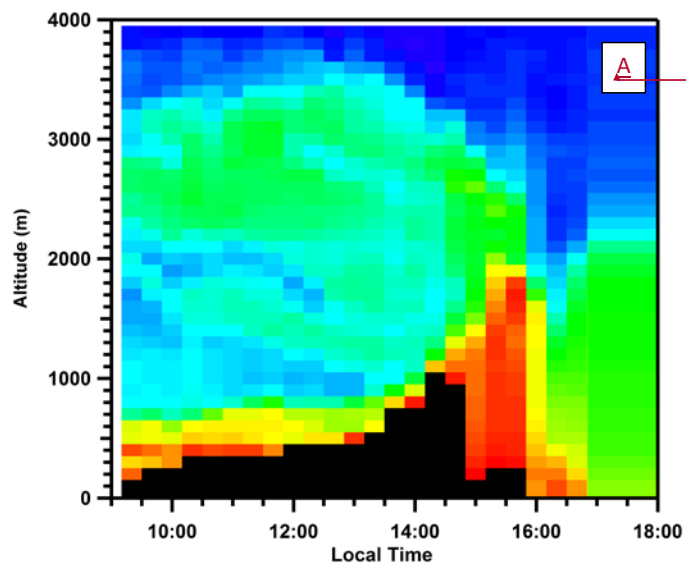


Figure S9 Averaged lidar profiles of aerosol extinction at 361 nm from 0-4 km from Sep 04 (A_{top}) and Aug 23 with S-ratio= 44 sr after 14:00 local time (B_{bottom}). Black indicates aerosol extinction values > 0.06.

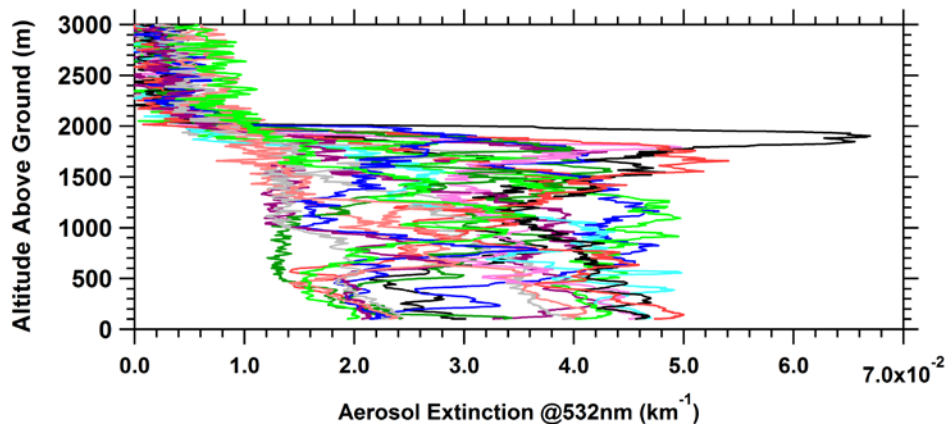


Figure S10 Variability in lidar vertical profiles of aerosol extinction from 15:27 to 15:37 local time on Sep 07.

Section 7 WBEA In-Situ Measurements of SO₂ and NO₂ at Fort McKay South and Fort McKay Sites

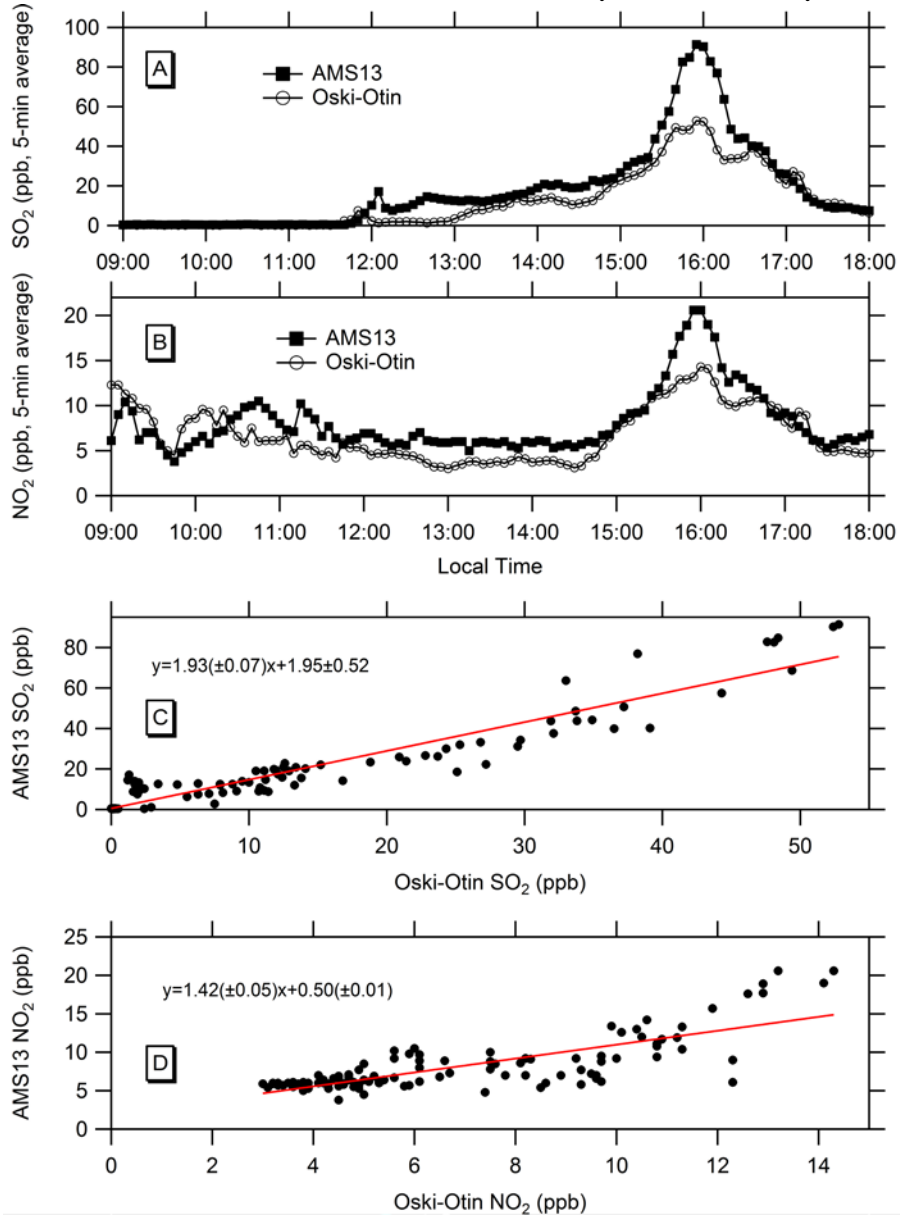


Figure S11 Aug 23 Time series of 5-minute average mixing ratios of SO₂ (A) and NO₂ (B) at Fort McKay South and Oski-Otin and linear regression scatter plots for SO₂ (C) and NO₂ (D).

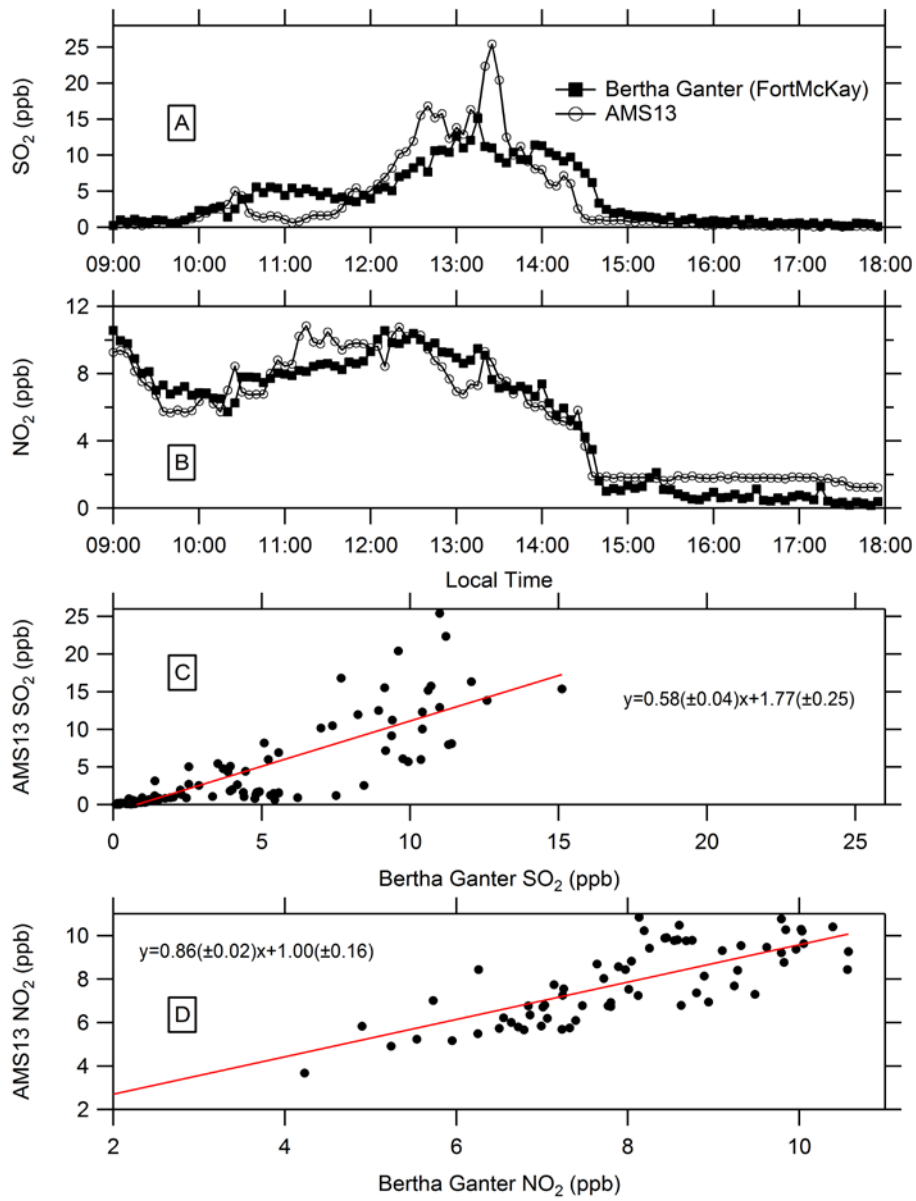


Figure S12 Sep 04 Time series of 5-minute average mixing ratios of SO₂ (A) and NO₂ (B) at Fort McKay South and Oski-Ôtin and linear regression scatter plots for SO₂ (C) and NO₂ (D).

Section 8 Further Information on Optimal Estimation Retrievals and Sensitivity Studies of A-Priori Shape

8.1 Quality Analysis of Retrievals

Typical degrees of freedom of signal were 1.6-2.1 and 2.3-3.0 for the aerosol and trace-gas retrievals, respectively.

Linear regressions in Tables S10 and S11 were computed using the retrieved (modelled) dSCD as the y-variable and the measured dSCD as the x-variable.

Table S10 Linear regression statistics for O₄ measured and retrieval modelled dSCDs.

Date	Species	Slope	R ²	N
23-Aug	O ₄	0.99	0.98	154
03-Sep	O ₄	0.99	0.91	109
04-Sep	O ₄	0.99	0.98	199
05-Sep	O ₄	0.99	0.98	181
06-Sep	O ₄	0.99	0.98	159
07-Sep	O ₄	0.99	0.96	178

Table S11 Linear regression statistics for SO₂ and NO₂ measured and retrieval modelled dSCDs.

Date	Species	Slope	R ²	N	Notes
23-Aug	SO ₂	0.99	0.98	154	
23-Aug	NO ₂	0.99	0.97	154	
03-Sep	SO ₂	0.90	0.69	109	
03-Sep	NO ₂	0.93	0.78	109	
04-Sep	SO ₂	0.97	0.91	199	
04-Sep	NO ₂	0.99	0.98	199	
05-Sep	SO ₂	0.49	-0.50	181	Many zero within error measured dSCD values
05-Sep	NO ₂	0.93	0.59	181	Many zero within error measured dSCD values
06-Sep	SO ₂	0.82	0.77	159	Very small SO ₂ dSCDs
06-Sep	NO ₂	1.00	0.99	159	
07-Sep	SO ₂	0.90	0.67	178	Rapidly varying vertical profiles
07-Sep	NO ₂	0.90	0.73	178	Rapidly varying vertical profiles

The modelled and measured O₄ exhibited strong agreement (slope=0.99 and R²>0.91) for all days (Table S10). The trace-gas dSCDs showed good agreement (slope>0.9 and R²>0.9) for Aug 23, Sep 04 and Sep 06 (NO₂ only). The Sep 06 dSCDs of SO₂ showed slightly weaker agreement (slope=0.82 and R²=0.77) due to relatively low values of SO₂ dSCDs, including many zero within error values for the 15° and 30° elevation angle measurements. The Sep 05 trace-gas correlations were weak due to clean pollution conditions leading to many measured dSCDs values that were zero within error. The correlation strength of the Sep 03 trace-gas dSCDs is relatively weak (R²= 69-7878), potentially due to the complexity of the vertical profiles from the observed wind-shear (Fig. 3 (B)). The Sep 07 trace-gas dSCDs had relatively weaker correlation strengths (R²=0.67-0.73), likely due to the rapidly varying vertical profiles of pollution resulting in different dSCDs observing different air masses such that no profile shape could fit the data.

8.2 Sensitivity Case Studies

Formatted: Superscript

Formatted: Superscript

For each of the retrievals in the sensitivity study, only one parameter of the a-priori shape was altered with all other retrieval settings were the same as described in section 2.3.2. All sensitivity retrievals are compared to the “base-case” of an exponentially decreasing a-priori profile with scale height of 0.6 km.

8.2.1 Measured versus Modelled dSCDs

Table S12 Linear regression statistics for O₄ measured and retrieval modelled dSCDs from the base case (exponential shape) a-priori against other a-priori shapes. The retrieved (modelled) dSCD was the y-variable and the measured dSCD was the x-variable.

Date	Species	A-priori	Slope	R ²	N
23-Aug	O ₄	Exponential	0.99	0.97	193.00
23-Aug	O ₄	Gaussian	0.99	0.96	193.00
23-Aug	O ₄	Boltzmann	0.99	0.98	193.00
23-Aug	O ₄	h=0.3km	0.99	0.97	193.00
23-Aug	O ₄	h=1.2 km	0.99	0.97	193.00

Table S13 Linear regression statistics for SO₂ measured and retrieval modelled dSCDs from the base case (exponentially shaped) a-priori against other a-priori shapes. The retrieved (modelled) dSCD was the y-variable and the measured dSCD was the x-variable.

Date	Species	A-priori	Slope	R ²	N
23-Aug	SO ₂	Exponential	0.99	0.98	193.00
23-Aug	SO ₂	Gaussian	0.99	0.97	193.00
23-Aug	SO ₂	Boltzmann	0.99	0.97	193.00
23-Aug	SO ₂	h=0.3 km	1.00	0.99	193.00
23-Aug	SO ₂	h=1.2 km	1.00	1.00	193.00

Table S14 Linear regression statistics for NO₂ measured and retrieval modelled dSCDs from the base case (exponentially shaped) a-priori against other a-priori shapes. The retrieved (modelled) dSCD was the y-variable and the measured dSCD was the x-variable.

Date	Species	A-priori	Slope	R ²	N
23-Aug	NO ₂	Exponential	0.99	0.97	193.00
23-Aug	NO ₂	Gaussian	0.99	0.97	193.00
23-Aug	NO ₂	Boltzmann	0.99	0.97	193.00
23-Aug	NO ₂	h=0.3 km	0.99	0.96	193.00
23-Aug	NO ₂	h=1.2 km	0.99	0.99	193.00

Table S15 Linear regression statistics for O₄ measured and retrieval modelled dSCDs from the base case (exponential shape) a-priori against other a-priori shapes. The retrieved (modelled) dSCD was the y-variable and the measured dSCD was the x-variable.

Date	Species	A-priori	Slope	R ²	N
04-Sep	O ₄	Exponential	0.99	0.98	199.00

04-Sep	O ₄	Gaussian	0.99	0.96	199.00
04-Sep	O ₄	Boltzmann	1.00	0.98	199.00
04-Sep	O ₄	h=0.3 km	1.00	0.98	199.00
04-Sep	O ₄	h=1.2 km	0.99	0.98	199.00

Table S16 Linear regression statistics for SO₂ measured and retrieval modelled dSCDs from the base case (exponentially shaped) a-priori against other a-priori shapes. The retrieved (modelled) dSCD was the y-variable and the measured dSCD was the x-variable.

Date	Species	A-priori	Slope	R ²	N
04-Sep	SO ₂	Exponential	0.97	0.91	199.00
04-Sep	SO ₂	Gaussian	0.97	0.90	199.00
04-Sep	SO ₂	Boltzmann	0.97	0.90	199.00
04-Sep	SO ₂	h=0.3 km	0.97	0.92	199.00
04-Sep	SO ₂	h=1.2 km	0.98	0.90	199.00

Table S17 Linear regression statistics for NO₂ measured and retrieval modelled dSCDs from the base case (exponentially shaped) a-priori against other a-priori shapes. The retrieved (modelled) dSCD was the y-variable and the measured dSCD was the x-variable.

Date	Species	A-priori	Slope	R ²	N
04-Sep	NO ₂	Exponential	0.99	0.98	199.00
04-Sep	NO ₂	Gaussian	0.99	0.97	199.00
04-Sep	NO ₂	Boltzmann	0.99	0.98	199.00
04-Sep	NO ₂	h=0.3 km	0.99	0.98	199.00
04-Sep	NO ₂	h=1.2 km	0.99	0.97	199.00

8.2.2 Comparison of AODs and VCDs from Base Case (Exponential) A-Priori and Other Shapes

Note that the x and y variables were the retrieval value from the exponential a-priori (base case) and other a-priori shape, respectively. The linear fit statistics were computed using the “linfitxy” function (Browaeys, 2017) in MATLAB using the respective errors retrieval by the optimal estimation inversion.

Table S18 Linear regression statistics of Aug 23 AODs retrieved using the exponential and other a-priori shapes.

Date	Variable	Shape	Slope	Slope Error	Intercept	Intercept Error	R ²
23-Aug	AOD	Gaussian	0.88	0.02	0.00	0.00	0.97
23-Aug	AOD	Boltzmann	0.92	0.01	0.00	0.00	0.99
23-Aug	AOD	h=0.3 km	0.79	0.01	0.00	0.00	0.94
23-Aug	AOD	h=1.2 km	0.92	0.03	-0.03	0.01	0.89

Table S19 Linear regression statistics of Aug 23 SO₂ VCDs retrieved using the exponential and other a-priori shapes.

<u>Date</u>	<u>Variable</u>	<u>Shape</u>	<u>Slope</u>	<u>Slope Error</u>	<u>Intercept (molec. cm⁻²)</u>	<u>Intercept Error</u>	<u>R²</u>
23-Aug	SO ₂ VCD	Gaussian	1.0	0.0	-2.11x10 ¹⁵	1.4x10 ¹⁵	0.99
23-Aug	SO ₂ VCD	Boltzmann	1.0	0.0	-1.11x10 ¹⁵	1.3x10 ¹⁵	0.99
23-Aug	SO ₂ VCD	h=0.3	0.8	0.0	1.77x10 ¹⁵	9.5x10 ¹⁴	0.97
23-Aug	SO ₂ VCD	h=1.2	1.2	0.0	-5.83x10 ¹⁴	2.1x10 ¹⁵	0.99

Table S20 Linear regression statistics of Aug 23 NO₂ VCDs retrieved using the exponential and other a-priori shapes.

<u>Date</u>	<u>Variable</u>	<u>Shape</u>	<u>Slope</u>	<u>Slope Error</u>	<u>Intercept (molec. cm⁻²)</u>	<u>Intercept Error</u>	<u>R²</u>
23-Aug	NO ₂ VCD	Gaussian	0.8	0.0	8.73x10 ¹⁴	2.7x10 ¹⁴	0.96
23-Aug	NO ₂ VCD	Boltzmann	0.9	0.0	6.57x10 ¹⁴	2.4x10 ¹⁴	0.97
23-Aug	NO ₂ VCD	h=0.3	0.7	0.0	9.05x10 ¹⁴	1.8x10 ¹⁴	0.89
23-Aug	NO ₂ VCD	h=1.2	1.2	0.0	-7.07x10 ¹⁴	4.4x10 ¹⁴	0.95

Table S21 Linear regression statistics of Sep 04 AODs retrieved using the exponential and other a-priori shapes.

<u>Date</u>	<u>Variable</u>	<u>Shape</u>	<u>Slope</u>	<u>Slope Error</u>	<u>Intercept</u>	<u>Intercept Error</u>	<u>R²</u>
04-Sep	AOD	Gaussian	0.76	0.08	0.02	0.01	0.68
04-Sep	AOD	Boltzmann	0.93	0.06	0.00	0.01	0.97
04-Sep	AOD	h=0.3 km	0.81	0.04	0.01	0.00	0.94
04-Sep	AOD	h=1.2 km	1.14	0.13	0.00	0.01	0.95

Table S22 Linear regression statistics of Sep 04 SO₂ VCDs retrieved using the exponential and other a-priori shapes.

<u>Date</u>	<u>Variable</u>	<u>Shape</u>	<u>Slope</u>	<u>Slope Error</u>	<u>Intercept (molec. cm⁻²)</u>	<u>Intercept Error</u>	<u>R²</u>
04-Sep	SO ₂ VCD	Gaussian	1.05	0.25	-1.49x10 ¹⁵	3.23x10 ¹⁵	0.98
04-Sep	SO ₂ VCD	Boltzmann	1.02	0.22	-1.16x10 ¹⁵	2.94x10 ¹⁵	0.98
04-Sep	SO ₂ VCD	h=0.3 km	0.99	0.17	-1.83x10 ¹⁵	2.24x10 ¹⁵	0.99
04-Sep	SO ₂ VCD	h=1.2 km	1.17	0.35	2.43x10 ¹⁵	4.59x10 ¹⁵	0.97

Table S23 Linear regression statistics of Sep04 NO₂ VCDs retrieved using the exponential and other a-priori shapes.

<u>Date</u>	<u>Variable</u>	<u>Shape</u>	<u>Slope</u>	<u>Slope Error</u>	<u>Intercept (molec. cm⁻²)</u>	<u>Intercept Error</u>	<u>R²</u>
-------------	-----------------	--------------	--------------	--------------------	---	------------------------	----------------------

04-Sep	NO ₂ VCD	Gaussian	1.00	0.12	-2.82x10 ¹⁴	8.24x10 ¹⁴	0.98
04-Sep	NO ₂ VCD	Boltzmann	0.98	0.11	-2.17x10 ¹⁴	7.64x10 ¹⁴	0.99
04-Sep	NO ₂ VCD	h=0.3 km	0.92	0.09	-1.92x10 ¹⁴	5.69x10 ¹⁴	0.98
04-Sep	NO ₂ VCD	h=1.2 km	1.17	0.17	-1.55x10 ¹⁴	1.17x10 ¹⁵	0.96

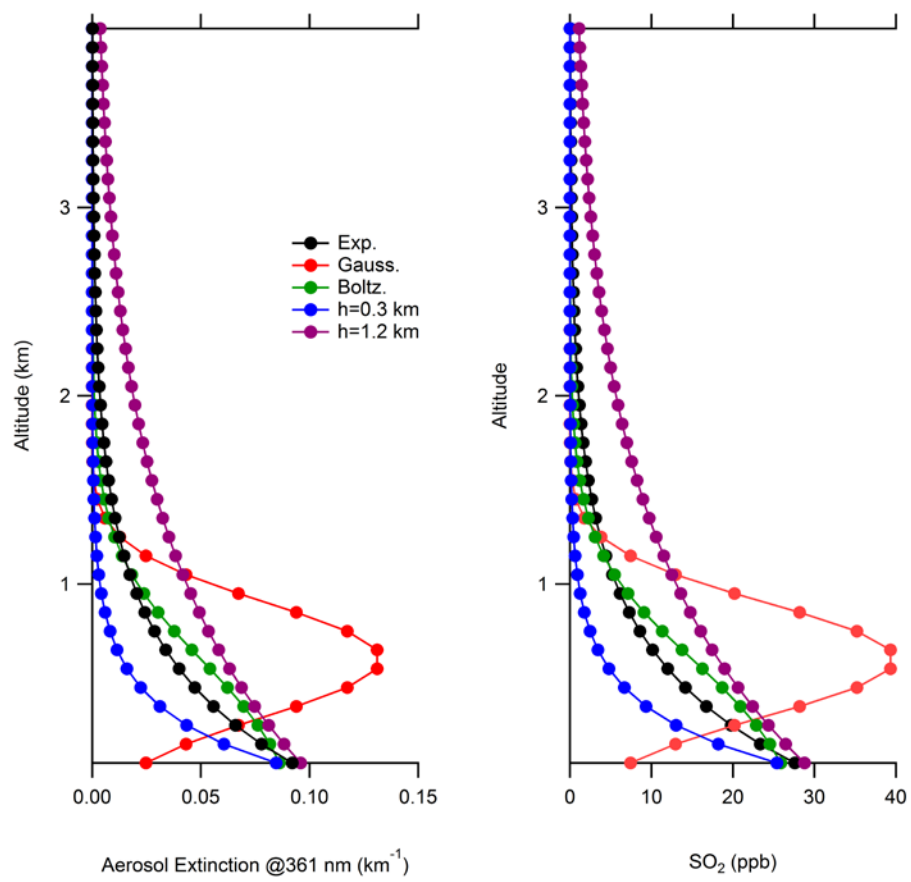


Figure S13 A-priori shapes for sensitivity tests of retrievals of aerosol extinction (left) and SO₂ (right).

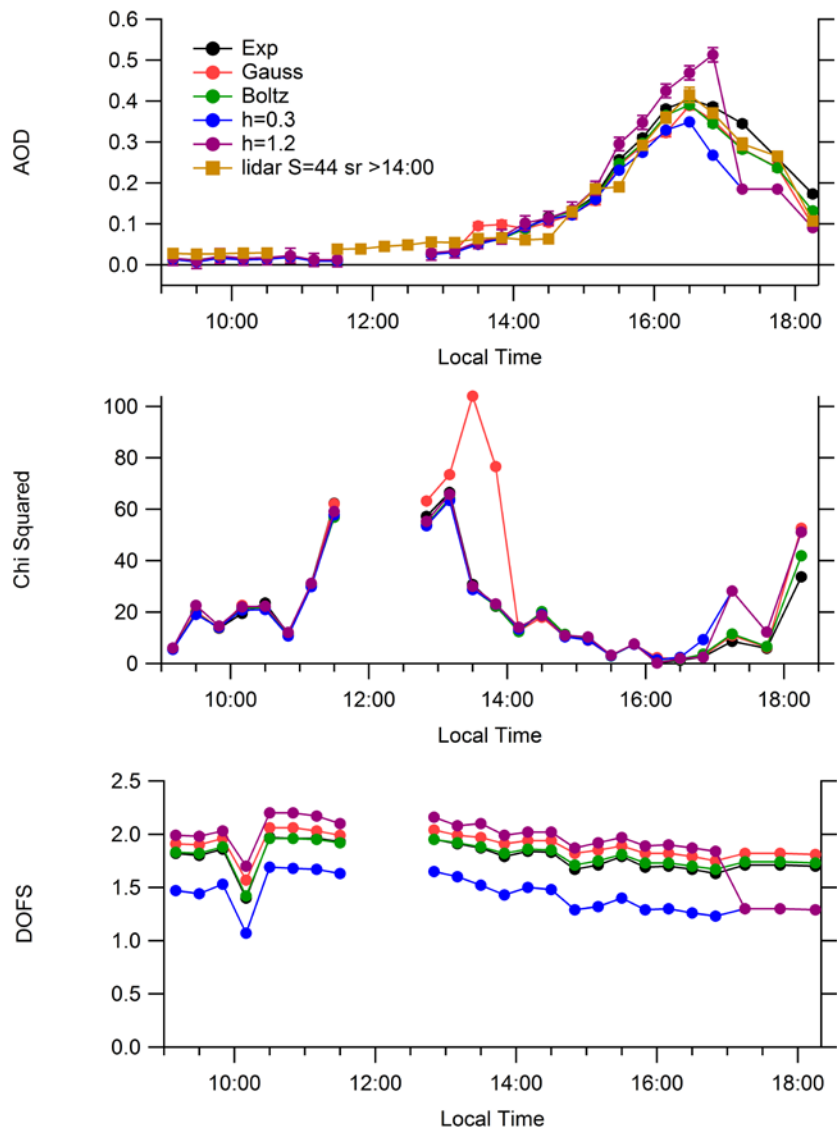


Figure S14 Aug 23 aerosol retrieval a-priori sensitivity studies of AOD (with smoothed lidar AOD also shown), Chi Squared and degrees of freedom of signal (DOFS).

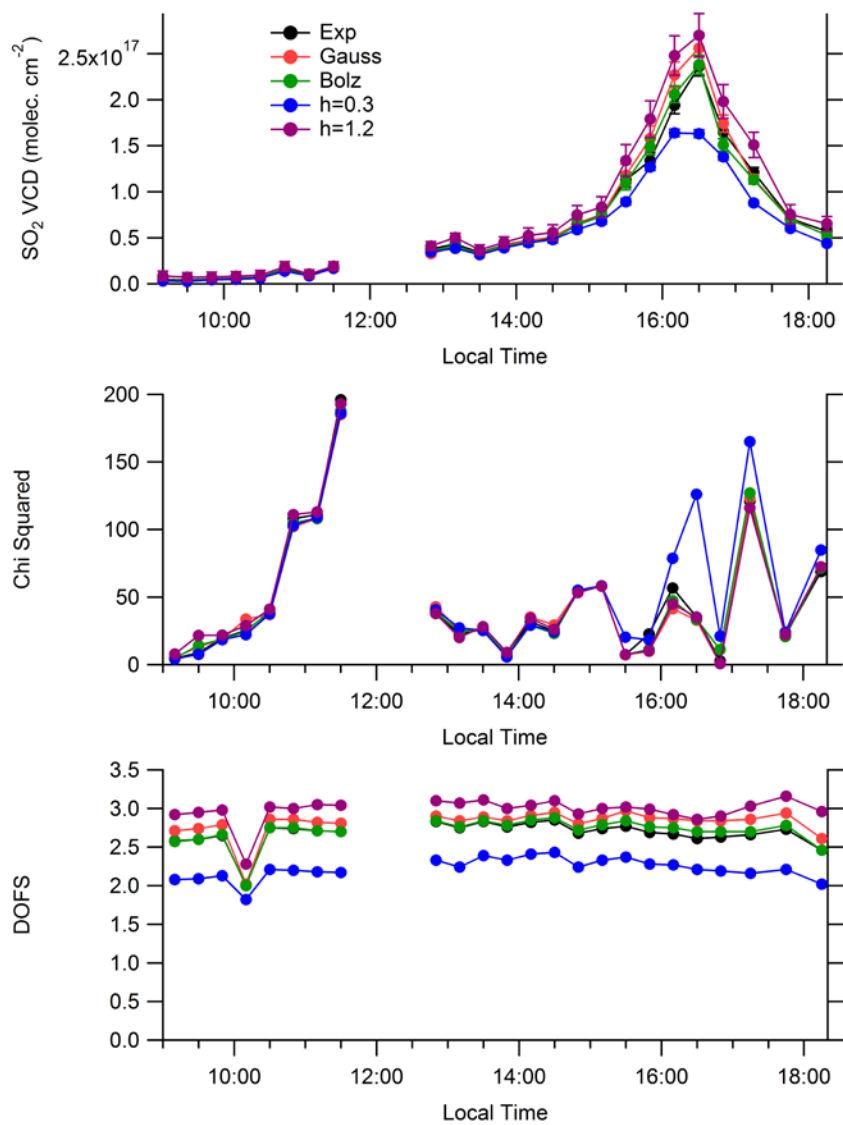


Figure S15 Aug 23 SO₂ retrieval a-priori sensitivity studies of SO₂ VCD, Chi Squared and degrees of freedom of signal (DOFS).

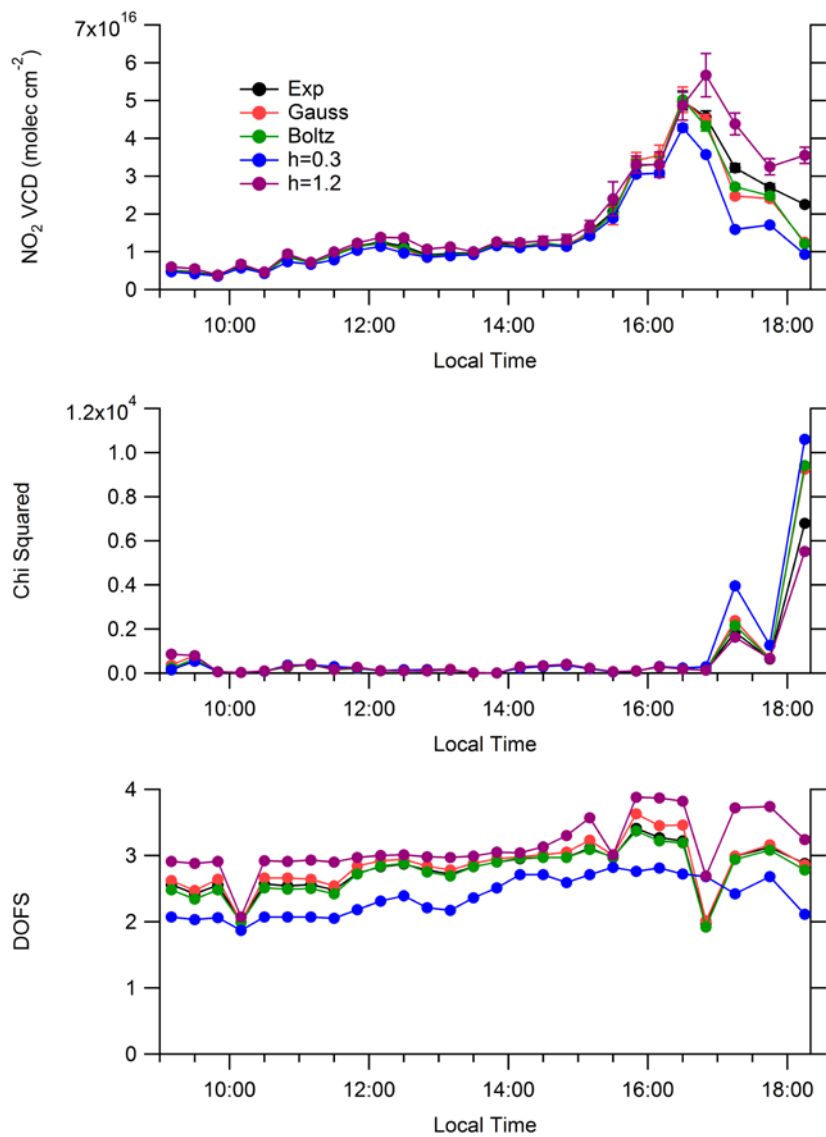


Figure S16 Aug 23 NO₂ retrieval a-priori sensitivity studies of NO₂ VCD, Chi Squared and degrees of freedom of signal (DOFS).

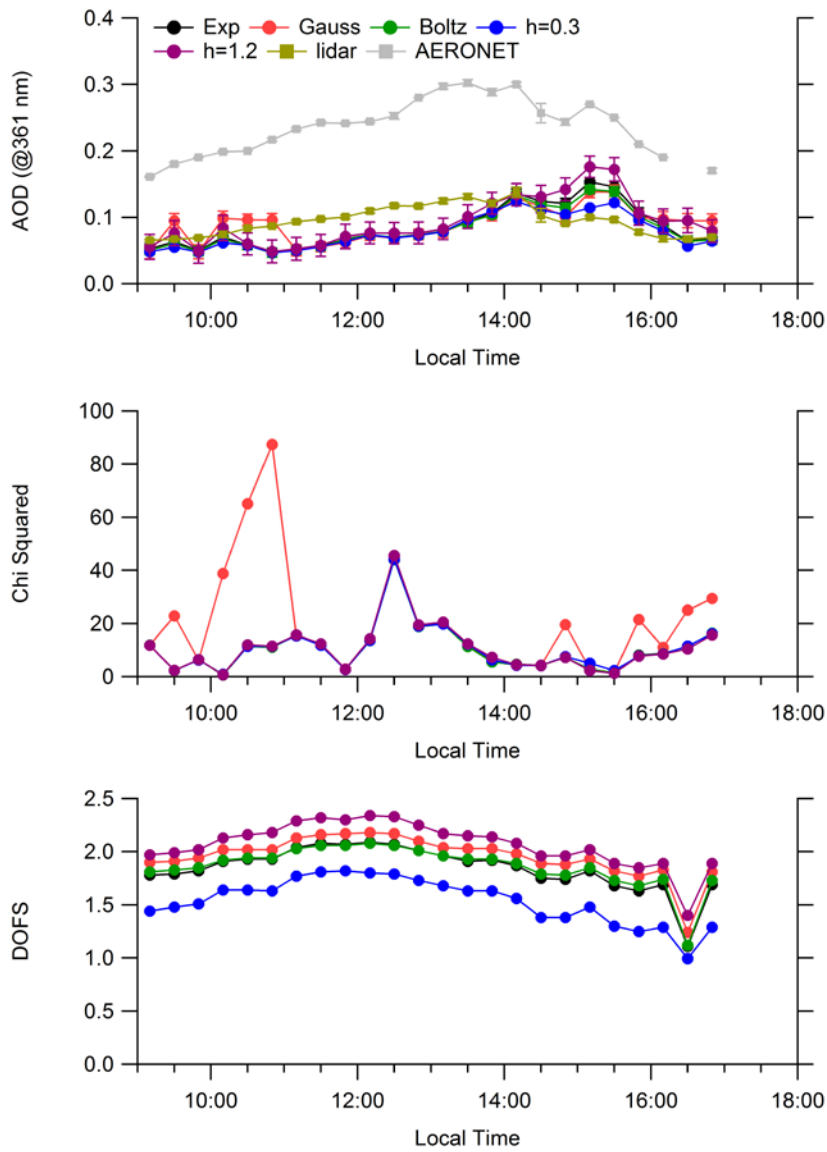


Figure S17 Sep 04 aerosol retrieval a-priori sensitivity studies of AOD (lidar and AERONET also shown), Chi Squared and degrees of freedom of signal (DOFS).

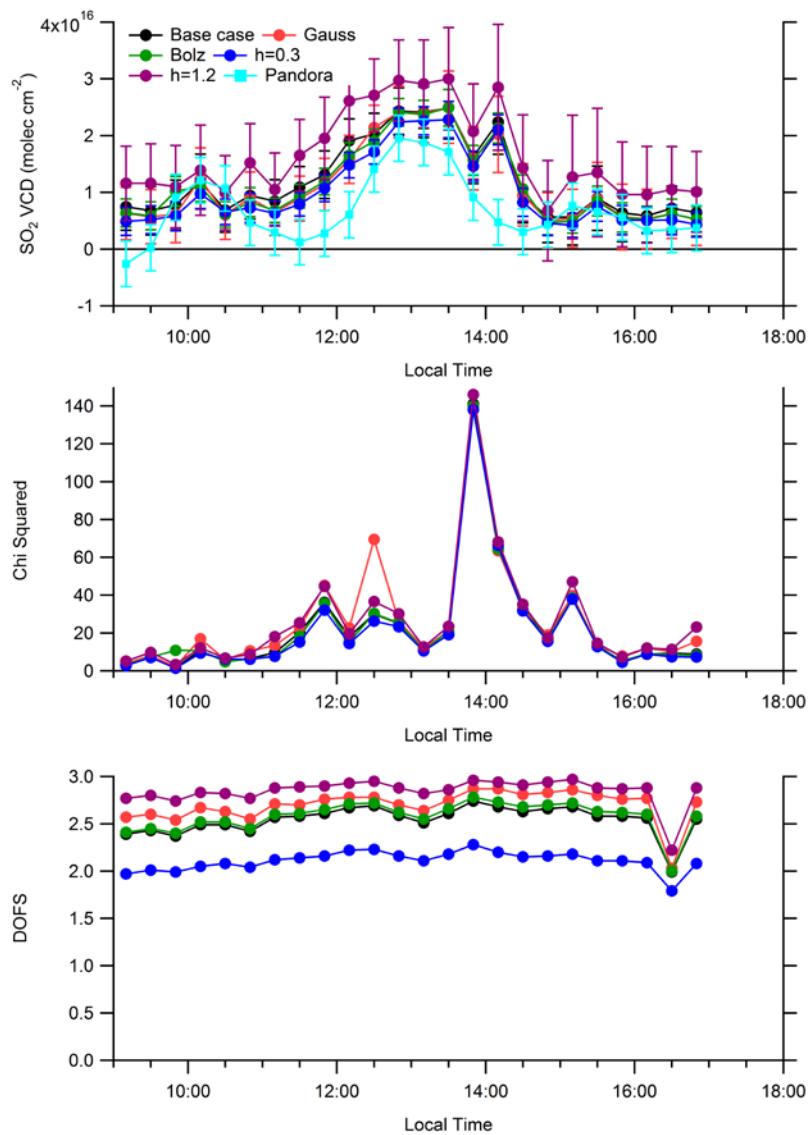


Figure S18 Sep 04 SO₂ retrieval a-priori sensitivity studies of SO₂ VCD (Pandora VCDs also shown), Chi Squared and degrees of freedom of signal (DOFS).

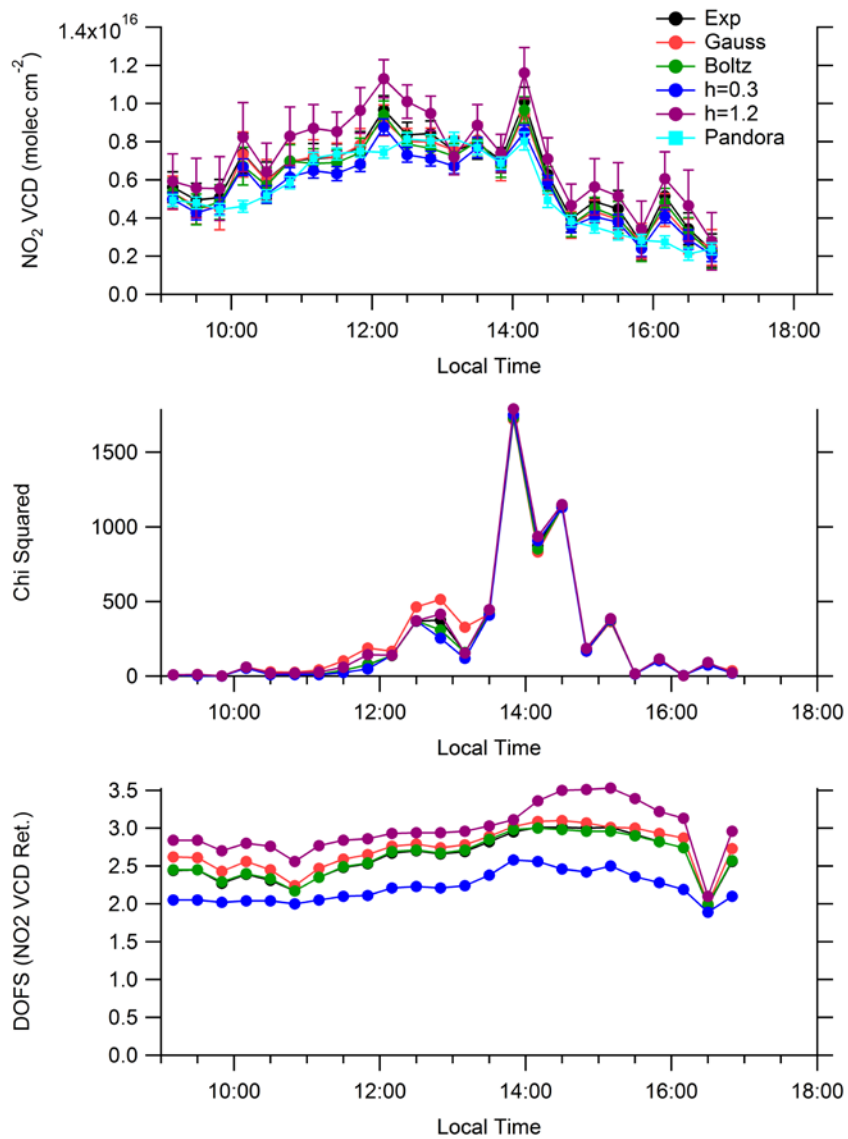


Figure S20 Sep 04 NO₂ retrieval a-priori sensitivity studies of NO₂ VCD (Pandora VCDs also shown), Chi Squared and degrees of freedom of signal (DOFS).

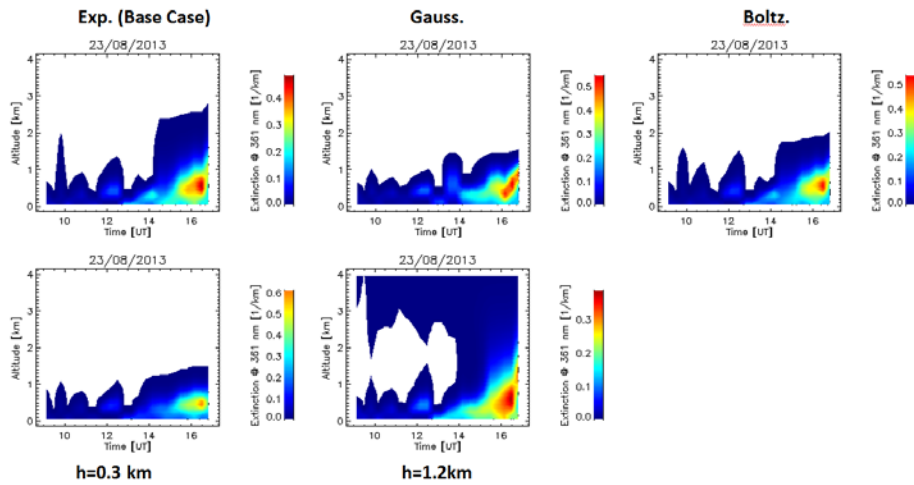


Fig S21 Aug 23 aerosol extinction retrievals using the five a-priori shapes. Note the difference in scale maximum values.

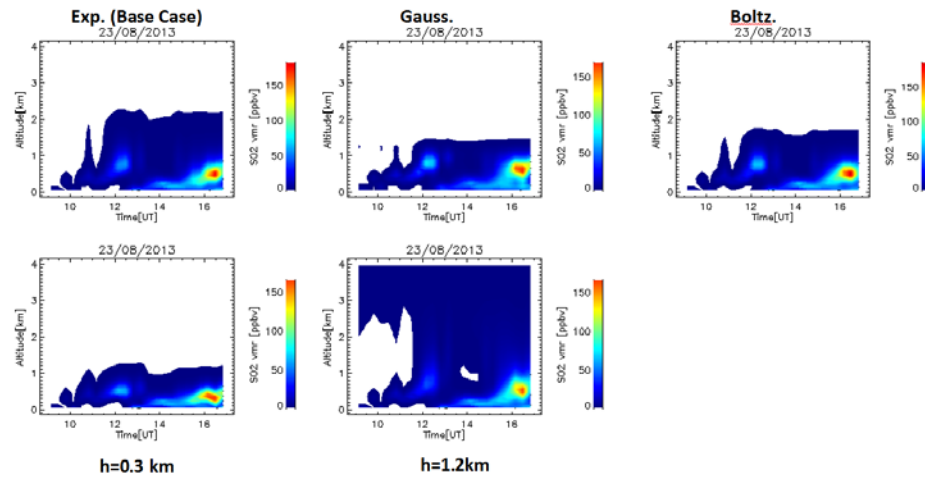


Fig S22 Aug 23 SO₂ retrievals using the five a-priori shapes. Note the difference in scale maximum values.

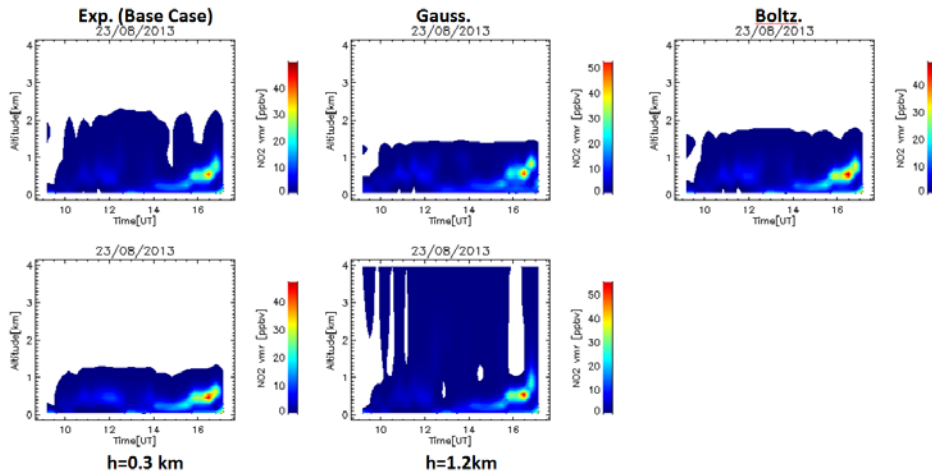


Fig S23 Aug 23 NO_2 retrievals using the five a-priori shapes. Note the difference in scale maximum values.

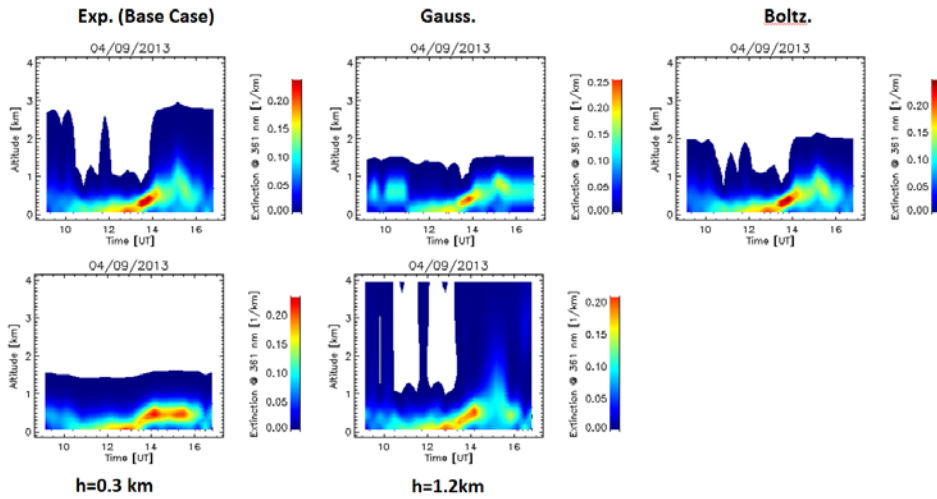


Fig S24 Sep04 aerosol extinction retrievals using the five a-priori shapes. Note the difference in scale maximum values.

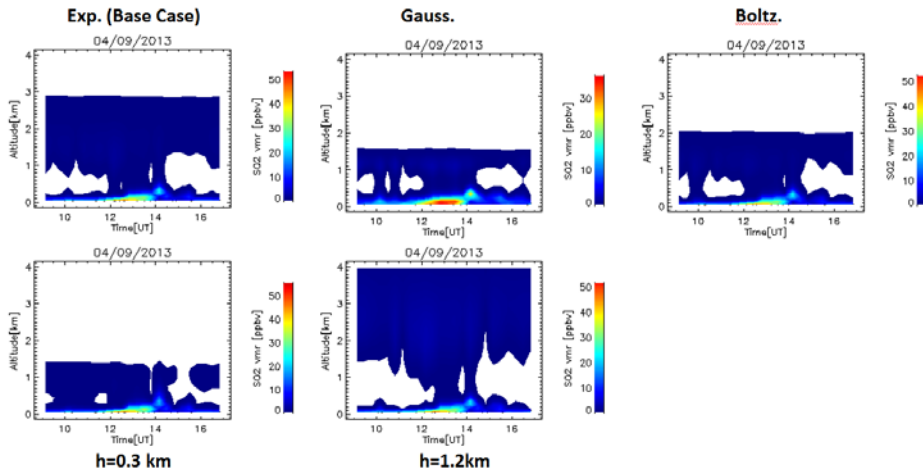


Fig S24 Sep04 SO₂ retrievals using the five a-priori shapes. Note the difference in scale maximum values.

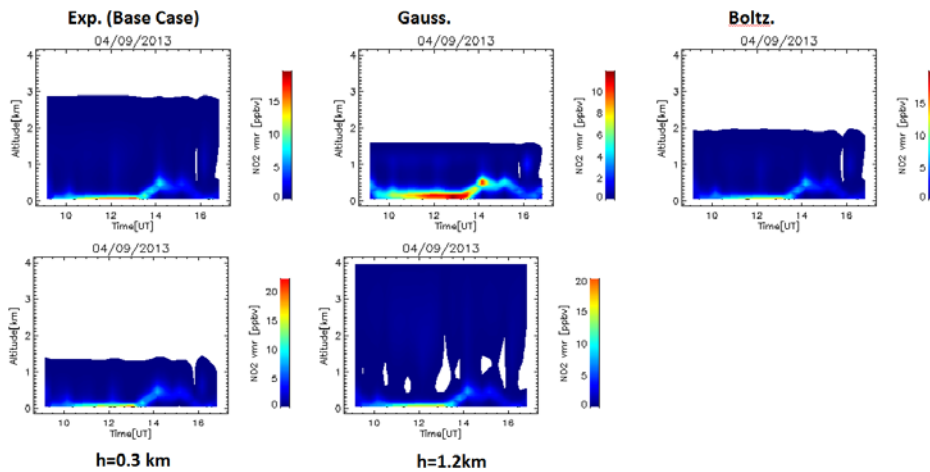


Fig S25 Sep04 NO₂ retrievals using the five a-priori shapes. Note the difference in scale maximum values.

There was little variation in the slope and coefficient of determination (R^2) of the linear regression of modelled and measured dSCDs between the five a-priori shapes (Tables S12-S17). For all a-priori shapes, $R^2 > 0.90$ and the slope was between 0.97 and 1.0. For both days, the R^2 changed by up to 0.3 between the five shapes.

The SO₂ VCDs from the different a-priori profiles tended to be equal within error when $< 1 \times 10^{17}$ molec. cm⁻² and NO₂ VCDs tended to be equal within error when $< 4 \times 10^{16}$ molec. cm⁻² due to larger error to value ratios (Figs. S15-S16 & S18-S19). Consequently, the Sep 04 trace-gas VCDs from the five different a-priori shapes were statistically

equal within error (Tables S22 & S23, Figs. S18-S19). The Aug 23 VCDs were statistically different during the afternoon where the h=1.2 km and h= 0.3 km retrievals produce the greatest and smallest VCDs that were ~20% greater than and less than the “base-case” exponential retrievals, respectively.

The Gaussian a-priori profile shape was not used for the retrievals because sensitivity studies indicated that this profile sometimes resulted in retrieved AODs or VCDs that appeared to be outliers compared to the other four shapes. The associated chi-squared (cost function) values of the Gaussian a-priori retrievals were greater than those of all the other shapes (Figs. S14, & S17-20). For example, the Sep 04 Gaussian a-priori AODs increased during 10:00-11:00 compared to the other shapes with a cost function up to ten times greater; note that this temporal trend was not reflected in the lidar or AERONET AODs (Fig. S17). Using the Gaussian shaped a-priori may have resulted in instability in the retrievals, potentially due to too much freedom at higher altitudes compared to the other profiles (Fig. S13).

The Boltzmann and “base-case” exponential retrieved AODs were within +/-10%.

The a-priori with a scale height of 0.3 km decreased the AODs or VCD retrievals by 0-30% compared to the “base-case”, depending on the day and species (Tables S18-S23). The retrievals using this a-priori resulted in greater chi-squared values for the h= 0.3 profiles compared to the other profiles for some retrievals after 15:00 (Figs. S14-S16). This smaller a-priori scale height was not used for the retrievals because it was probably too restrictive in terms of the decrease in the a-priori values profile values between ~0.5-1 km under well-mixed, afternoon boundary layer conditions.

The a-priori with a scale height of 1.2 km increased the AOD or VCD retrieved values by ~20% compared to the “base-case”, generally because there was little information content from the MAX-DOAS measurements above ~1.5 km and the retrieval reverted to the non-zero a-priori values (Figs. S21-S25). Consequently, this profile shape increased the proportion of aerosol extinction and trace-gas concentration present at >2 km altitude to the 0-4 km column value (Figs. S21-S25). For some of the vertical profiles on both days, the retrieval reduced the aerosol extinction to zero by ~1 km but this a-priori resulted in non-zero values at 2-4 km (Figs. S21-S25). This larger scale height was not used for the retrievals because it resulted in non-zero values at high altitudes where there was little to no information content from the measurements (Figs. S7, S21-S25). Since the values at these higher altitudes were unknown and likely varied temporally, a scale height that allowed the values to be retrieved at zero was chosen (i.e., h= 0.6 km). An a-priori scale height that resulted in underestimated rather than overestimated retrievals of the pollution loading where there was a lack of information content was considered preferable.